Triplet 4*d* states of H_2: Experimental observation and comparison with an *ab initio* model for Rydberg-state energies

E. E. Eyler and F. M. Pipkin
Lyman Laboratory of Physics, Harvard University, Cambridge, Massachusetts 02138
(Received 18 October 1982)

The triplet 4*d* states of H_2 have been studied by using a tunable single-mode dye laser to excite metastable molecules in the $2p\ ^3\Pi_u$ state to the 4*s* and 4*d* triplet states. Ninety-three transitions were detected and their line positions measured. Some of these states decay primarily by predissociation. A simple model for the energies of the Rydberg states was developed; the model depends upon the polarizability and quadrupole interactions of the Rydberg electron with the H_2^+ core. It provides a remarkably good description of the measured energy intervals.

I. INTRODUCTION

The first extensive measurements of the triplet states of the hydrogen molecule were made in the 1930s by Richardson and his co-workers.[1–3] Among other things they observed the transitions from the triplet 4*d* states to the metastable $c\ ^3\Pi_u\ 2p\pi$ state and used these observations to determine the energy levels for the triplet 4*d* states. In the 1950s Dieke and his co-workers obtained spectra with higher resolution and improved the assignments of the energy levels.[4] Neither of these groups was able to identify transitions from the triplet 4*s* state and thus determine its energy levels. This paper reports the first improvement in the optical spectroscopy of these states since that time.

Spectra of very high resolution and selectivity have been obtained by using a tunable single-mode dye laser to excite transitions in a collimated beam of metastable hydrogen molecules. Only those transitions in the blue region of the spectrum terminating with the triplet 4*s* and 4*d* states were observed; this made the identification process far easier than for the emission spectra upon which earlier investigators relied. A number of errors in the earlier identifications have been discovered. In particular, it has been necessary to revise nearly all the energy levels with $v=2$. This paper will focus on the 4*d* states, although some discussion of the $4s\ ^3\Sigma_g^+$ state is necessary in describing the process through which the lines were identified. The properties of the 4*s* state are described in another publication.[5]

As an aid in understanding and identifying the levels a simple model for the energies of the Rydberg states has been developed, based upon the polarizability and quadrupole interactions of the Rydberg electron with the H_2^+ core. This model gives results that agree remarkably well with the experimental energies. A similar analysis has been applied to the Rydberg states of atomic C, N, O, and Ne by Chang and Sakai,[6] also with good results. Very recently Herzberg and Jungen have identified several $5g \rightarrow 4f$ transitions in the optical emission spectrum of H_2 by using a similar model.[7] The approach presented here is equivalent in principle, but differs in starting from a case-*d* basis set in which the energies are nearly diagonal.

The laser-molecular beam arrangement has also made it possible to study predissociation in the 4*s*,4*d* complex. There is an extensive literature on the competition between predissociation, autoionization, and radiative decay for the singlet *p* states of H_2.[8–11] Evidence for predissociation has been found for many of the lower Rydberg states, usually in the form of spectral broadening resulting from very short decay lifetimes. The $n=4$ states are energetically capable of predissociation for $v \geq 1$. It has been found that predissociation takes place for the 4*s* and 4*d* states with $v \geq 2$, although the $v=1$ levels appear in all cases to decay purely radiatively. The predissociative levels are detected via the Lyman-α radiation emitted by the excited H atoms resulting from the decay. The observed predissociation lifetimes vary erratically from about 100 psec to about 1 nsec, suggesting that the process is only weakly allowed for these states.

The first part of this paper describes the model and the calculation of the energy levels for the 4*d* states. Subsequent sections deal with the observation of the 4*s* and 4*d* states, the line assignments, and the comparison of the energy levels with the theory.

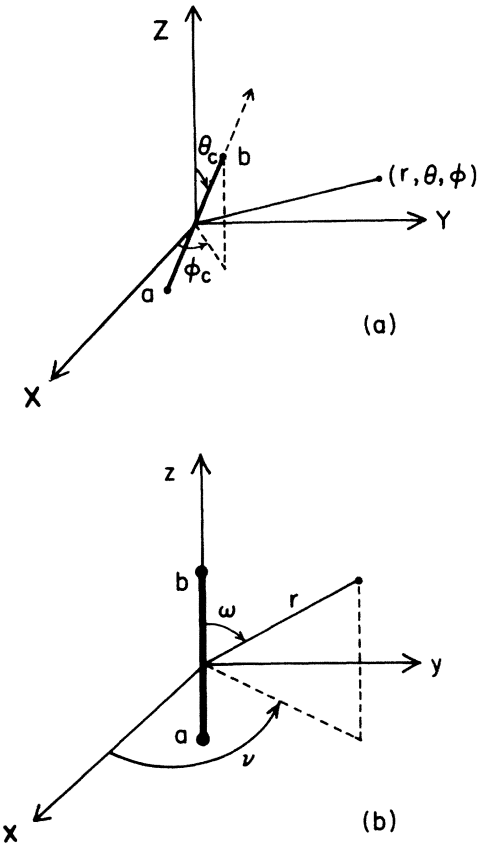

FIG. 1. Diagrams showing (a) the laboratory-fixed and (b) the molecule-fixed coordinate systems used to describe the hydrogen molecule.

II. STRUCTURE OF THE RYDBERG STATES OF H_2

A. Notation

This paper follows the notation used by Hougen.[12] $\vec{R}$ represents the rotational angular momentum of the molecule, $\vec{L}$ the orbital angular momentum of the excited electron, $\vec{S}$ the electronic-spin angular momentum, and $\vec{I}$ the nuclear-spin angular momentum. In describing the molecule, it is convenient to use both a frame of reference that is fixed in the laboratory and one that is fixed with respect to the molecule. Figure 1 shows the coordinates of one of the two electrons in each of these two systems. In the laboratory-fixed coordinate system [Fig. 1(a)] the origin for the coordinates is the center of mass of the two nuclei, the coordinates θ_c and ϕ_c define the orientation of the internuclear axis, and the polar coordinates (r,θ,ψ) define the position of the Rydberg electron. In the molecule-fixed frame the origin for the coordinates x,y,z is once more the center of mass of the molecule, the z axis points along the internuclear axis ab, and the position of the electron is defined by the polar coordinates (r,ω,ν).

B. Qualitative structure

Two angular momentum coupling schemes are important for the study of H_2, and some degree of intermediate coupling is usually encountered. The lowest excited states conform closely to Hund's case *b*, shown in Fig. 2(a). In this coupling scheme the electronic orbital angular momentum $\vec{L}$ is coupled strongly to the molecular core, so that its projection Λ along the internuclear axis ab is a good quantum number. The state is referred to by one of the Greek letters Σ, Π, Δ, Φ, . . . for $\Lambda=0$, 1, 2, 3, . . . The core rotational momentum $\vec{R}$ is well defined, but of little importance in describing levels. Instead the rotational levels are indexed according to N, the quantum number describing the total angular momentum exclusive of spin. The fine structure is included by coupling the electronic-spin angular momentum $\vec{S}$ with $\vec{N}$ to form $\vec{J}$, and the hyperfine structure by coupling the nuclear spin $\vec{I}$ to form $\vec{F}$.

As n and l increase, the system takes on the character of a hydrogenic Rydberg electron orbiting an H_2^+ core, interacting primarily with a central Coulomb potential. This corresponds to Hund's coupling case *d* and will be the starting point for the theoretical treatment that follows. Figure 2(b) shows the very simple case-*d* couplings, with $\vec{R}+\vec{L}$ forming $\vec{N}$, $\vec{N}+\vec{S}$ forming $\vec{J}$, and $\vec{J}+\vec{I}$ forming $\vec{F}$. The symmetries of a singly excited level in case *d* are easily found. The *gerade-ungerade* distinction is determined by L alone, with states of odd L having *ungerade* (u) symmetry. The "*s*", "*a*" symmetry (corresponding to laboratory-fixed permutation of the two nuclei) is determined by the core rotation alone. Levels of even R are parahydrogen levels and levels of odd R are orthohydrogen with a threefold hyperfine splitting. The structure of a case-*d* state

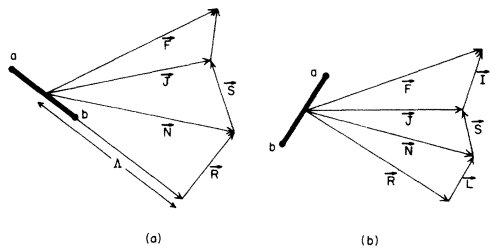

FIG. 2. Schematic diagram showing the two important angular momentum coupling schemes. (a) Hund's case *b*; (b) Hund's case *d*.

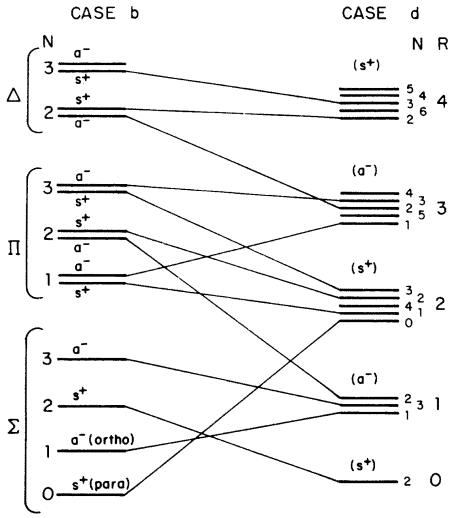

FIG. 3. Correlation diagram for a triplet d complex, showing the first few rotational levels for each state. Rotational spacings are not drawn to scale. Ordering shown for the N levels in case d is as calculated from Eq. (11). When corrected for off-diagonal terms, ordering for $N-R=0$ and $N-R=1$ is reversed for the nd states with $R=2$, 3, and 4.

consists of an "L complex" at each value of the rotational quantum number R with $2L+1$ closely spaced sublevels of different N when $R>L$. In unperturbed case d, these sublevels would be exactly degenerate. The rotational energy is given approximately by $BR(R+1)$, and the rotational constant B is expected to be close to that of the H_2^+ molecular ion.

To provide a qualitative understanding of the level structure for a state with intermediate coupling, the structures in the two coupling cases can be adiabatically connected. Figure 3 shows the correlation diagram for a d complex. It is constructed by conserving molecular symmetries and the quantum number N, which is always well defined. As the core coupling decreases (a phenomenon often referred to as "l uncoupling"), the two sublevels of opposite symmetry for each N are split further and further apart until they finally end up in quite different R levels. While the $3s,3d$ complex is somewhere near the middle of the correlation diagram, it will be shown that the $4d$ states lie fairly close to the limit of pure case d.

C. Interactions determining structure in case d

In this section the lowest-order couplings that perturb the Rydberg electron from hydrogenic energies are considered in detail. Before breaking the Hamiltonian of the system into perturbative and zeroth-order parts, it is helpful to develop a case-d basis set more explicitly than was done above. The overall wave function in pure case d has the form,

$$\psi=\mathscr{A}[\psi_{\rm Ryd}(\psi_{\rm nucl}\psi_{\rm core})] .$$

In this expression $\mathscr{A}$ is an antisymmetrizing operator, and $\psi_{\rm Ryd}$ is a hydrogenic Rydberg wave function

$$\psi_{\rm Ryd}=Y_{M_L}^{L}(\theta,\phi)R_{n,L}(r) .$$

The remainder of the wave function is just the wave function of H_2^+, which is further subdivided into $\psi_{\rm core}$, which is the electronic wave function of H_2^+, and

$$\psi_{\rm nucl}=\psi_{\rm rot}\psi_{\rm vib}\approx Y_{M_R}^{R}(\theta_c,\phi_c)\psi_{\rm vib}(A) ,$$

where A is the internuclear separation. The effect of the antisymmetrizing operator is to give rise to the portion of the singlet-triplet splitting that arises from exchange energy. It will be dropped from this point on, since the effects of electronic spin will not be included in this simple model. The complete case-d basis set is obtained by coupling the various angular momentum states to give kets of the form

$$|v,R,n,L,N,M_N\rangle = \sum_{M,M_R}[\,|n,L,M\rangle\,|v,R,M_R\rangle\,|\psi_{\rm core}\rangle \times(RM_RLM\,|\,RLNM_N)] . \quad (1)$$

The Hamiltonian of the system can be divided naturally into a portion that gives rise to the energies of the basis states and a portion that causes perturbations between them. Denoting the two nuclei by a and b, the inner electron by 1, and the Rydberg electron by 2, the perturbation Hamiltonian is given by

$$\mathscr{H}_{\rm pert}=\left[\frac{e^2}{r_{12}}+\frac{e^2}{r_2}\right]-\left[\frac{e^2}{r_{2a}}+\frac{e^2}{r_{2b}}\right] .$$

The first expression is the "atomic" perturbation and gives the deviation of the excited states of helium from the corresponding hydrogenic energies. The second expression contains all of the "molecular" interactions, which depend on the fact that the internuclear separation A is finite. The effect of this perturbation Hamiltonian on the system can be approximated by considering the two largest effects.

(1) The potential experienced by the outer electron is expanded into a multipole series, in which the quadrupole moment of the H_2^+ core is the first nonzero term.

(2) Second-order effects (mixing of the core states due to the presence of the outer electron) are taken into account by considering the polarizability of the H_2^+ core.

All higher moments and higher-order polarizabilities are assumed to be small, and the effects of core penetration by the Rydberg electron are neglected.

These two couplings must be expressed in a form such that matrix elements between basis states of the form given in Eq. (1) can be evaluated. Both perturbations are dependent upon the orientation of the internuclear axis, so it is necessary to consider the transformation between the laboratory coordinate frame and the molecule-fixed frame.

In the absence of core penetration, the Hamiltonian for the interaction of the Rydberg electron with the core potential is given by a simple multipole expansion

$$\begin{aligned}\mathscr{H}_{\rm el} &= \sum_{\rm core} \frac{e_{\rm Ryd}e_{\rm core}}{|r-r_{\rm core}|}\ , \\ &= \sum_{{\rm core},l} e_{\rm Ryd}e_{\rm core}\frac{r_{\rm core}^{l}}{r_{\rm Ryd}^{l+1}}P_l(\cos\omega_{2-{\rm core}})\ ,\end{aligned} \tag{2}$$

where $\omega_{2-\rm core}$ is the angle between the Rydberg electron and any one of the core particles, and the sum is over the electron and two protons in the core. The interaction can be expressed in terms of the angles describing the orientation of the Rydberg electron by using the spherical-harmonic addition theorem. For this and all other angular momentum relations in this paper the notation of Edmonds[13] will be used. For the quadrupole term the result is

$$\begin{aligned}\mathscr{H}_{\rm quad} &= \sum_{{\rm core},q}(-1)^q e_{\rm Ryd}e_{\rm core}\frac{r_{\rm core}^2}{r^3} \\ &\quad\times C_q^{(2)}(\omega,\nu)C_{-q}^{(2)}(\omega_{\rm core},\nu_{\rm core})\ .\end{aligned} \tag{3}$$

Because the core charge distribution has a cylindrical symmetry around the z axis when averaged over the motion of the core electron, only the $q=0$ term is nonzero and (3) simplifies to

$$\begin{aligned}\mathscr{H}_{\rm quad} &= \sum_{\rm core} e_{\rm Ryd}e_{\rm core}\frac{r_{\rm core}^2}{r^3}C_0^{(2)}(\omega,\nu)C_0^{(2)}(\omega_{\rm core},\nu_{\rm core}) \\ &= -\frac{e}{r^3}C_0^{(2)}(\omega,\nu)Q\ ,\end{aligned}$$

where

$$Q=\sum_{\rm core} e_{\rm core}r_{\rm core}^2 C_0^{(2)}(\omega_{\rm core},\nu_{\rm core})\ . \tag{4}$$

The electronic charge e in (4) is now signless.

It remains to express the quadrupole interaction in the laboratory-fixed system so that its matrix elements can be taken. This can be done using another application of the spherical-harmonic addition theorem. The result can be expressed as a product of two spherical-harmonic tensors in the laboratory coordinate system,

$$\mathscr{H}_{\rm quad}=-\frac{e}{r^3}\overleftrightarrow{C}^{(2)}(\theta,\phi)\cdot\overleftrightarrow{C}^{(2)}(\theta_c,\phi_c)Q\ . \tag{5}$$

The Hamiltonian for the polarization interaction can be derived by a similar treatment and has been carried out for a similar case by MacAdam.[14] For a general anisotropic object the polarizability tensor is defined as

$$\alpha_{ij}=\left[\frac{\partial^2 W}{\partial E_i\partial E_j}\right]_{E=0}\ ,$$

where E is the applied electric field. The resulting Hamiltonian is

$$\mathscr{H}_{\rm pol}=-\tfrac{1}{2}\sum_{i,j}E_i\alpha_{ij}E_j\ , \tag{6}$$

where the units of the α_{ij} are now a_0^3. The polarizability tensor must exhibit the cylindrical symmetry of the H_2^+ core, so in the molecule-fixed coordinate system it must have the form

$$\alpha_{ij}=\begin{bmatrix}\alpha_\perp & 0 & 0\\ 0 & \alpha_{||} & 0\\ 0 & 0 & \alpha_{||}\end{bmatrix}\ .$$

The Hamiltonian for the interaction of the Rydberg electron with the polarizable core can be rewritten in a very simple form if the isotropic polarizability α and the anisotropic polarizability γ are defined according to

$$\alpha=(2\alpha_\perp+\alpha_{||})/3\ ,$$
$$\gamma=\alpha_{||}-\alpha_\perp\ .$$

Using a spherical-harmonic tensor to express the angular dependence, the Hamiltonian in the molecule-fixed frame is

$$\mathscr{H}_{\rm pol}=-\tfrac{1}{2}\alpha E^2-\tfrac{1}{3}\gamma E^2 C_0^{(2)}(\omega,\nu)\ .$$

Inserting the electric field of the Rydberg electron explicitly, and writing the result in laboratory-fixed coordinates, the polarization Hamiltonian becomes

$$\mathscr{H}_{\rm pol}=-\frac{1}{2}\alpha\frac{e^2}{r^4}-\frac{1}{3}\gamma\frac{e^2}{r^4}\overleftrightarrow{C}^{(2)}(\theta,\phi)\cdot\overleftrightarrow{C}^{(2)}(\theta_c,\phi_c)\ , \tag{7}$$

Equations (5) and (7) form the core of the model for Rydberg-state structure. It is somewhat surprising that these interactions alone will be found to account for nearly all of the difference between purely hydrogenic energies and the energy levels for the molecular $4d$ states.

D. Energies and perturbations for case *d*

In this section, the matrix elements of the polarizability and quadrupole moment perturbations are obtained in a case-d basis. Starting with the quadrupole interactions and assuming that the vibrational motion is separable, the general matrix element can be decomposed according to

$$\langle v'R'n'L'N'M_N' \mid \mathscr{H}_{\rm quad} \mid vRnLNM_N\rangle = -e\langle v'R' \mid Q(A) \mid vR\rangle\langle n'L' \mid r^{-3} \mid nL\rangle \times\langle R'L'N'M_N' \mid \overleftrightarrow{C}^{(2)}(\theta,\phi)\cdot\overleftrightarrow{C}^{(2)}(\theta_c,\phi_c) \mid RLNM_N\rangle\ . \tag{8}$$

The matrix element involving the spherical-harmonic tensors can be evaluated explicitly to give the result

$$\begin{aligned}&\langle v'R'n'L'N'M_N' \mid \mathscr{H}_{\rm quad} \mid vRnLNM_n\rangle \\ &=-e\langle v'R' \mid Q(A) \mid vR\rangle\langle n'L' \mid r^{-3} \mid nL\rangle(-1)^{L+R'+N}\begin{Bmatrix}N & R' & L'\\ 2 & L & R\end{Bmatrix}\delta_{N'N}\delta_{M_N'M_N} \\ &\times(-1)^{L'}[(2L'+1)(2L+1)]^{1/2}\begin{pmatrix}L' & 2 & L\\ 0 & 0 & 0\end{pmatrix}(-1)^{R'}[(2R'+1)(2R+1)]^{1/2}\begin{pmatrix}R' & 2 & R\\ 0 & 0 & 0\end{pmatrix}\ .\end{aligned} \tag{9}$$

The selection rules for this perturbation can be obtained directly from the properties of the 3-j symbols,

$$\Delta N=0\ ,\quad \Delta M_N=0\ ,\quad \Delta R=0,\pm2\ ,\quad \Delta L=0,\pm2\ .$$

It can be shown from the properties of the Laguerre polynomials that the perturbations with $\Delta L=\pm2$ vanish if $\Delta n=0$ because the radial matrix element of r^{-3} is zero, so the interaction only mixes states with different L between manifolds with different principal quantum numbers.

The matrix elements of the polarizability perturbation (7) are obtained without having to do any new work. The isotropic term is trivial, and the anisotropic term has the same tensorial form as the quadrupole interaction (although it has a different radial matrix element). The result is that

$$\begin{aligned}&\langle v'R'n'L'N'M_N' \mid \mathscr{H}_{\rm pol} \mid vRnLNM_N\rangle \\ &=-e^2\langle n'L' \mid r^{-4} \mid nL\rangle\left[\tfrac{1}{2}\langle v'R' \mid \alpha(A) \mid vR\rangle\delta_{L'L}\delta_{R'R}\right. \\ &\quad+\tfrac{1}{3}\langle v'R' \mid \gamma(A) \mid vR\rangle(-1)^{L+R'+N}\begin{Bmatrix}N & R' & L'\\ 2 & L & R\end{Bmatrix}\delta_{N'N}\delta_{M_N'M_N} \\ &\quad\times(-1)^{L'}[(2L'+1)(2L+1)]^{1/2}\begin{pmatrix}L' & 2 & L\\ 0 & 0 & 0\end{pmatrix} \\ &\quad\left.\times(-1)^{R'}[(2R'+1)(2R+1)]^{1/2}\begin{pmatrix}R' & 2 & R\\ 0 & 0 & 0\end{pmatrix}\right]\ .\end{aligned} \tag{10}$$

The selection rules are the same as those for the quadrupole interaction, except that the polarizability is permitted to mix states with $\Delta L=\pm2$ even within the same principal quantum number manifold.

Equations (9) and (10) contain all of the physics of the model. To obtain the first-order energy corrections it is necessary only to specialize these expressions for the case where the matrix elements are diagonal in all quantum numbers. After writing out the values of the 3-j and 6-j symbols explicitly, the correction to the hydrogenic energy is found to be

$$E^{(0)}=-\frac{e}{a_0^3}\langle vR\mid Q(A)\mid vR\rangle\frac{1}{n^3(L+1)(L+\frac{1}{2})L}\frac{3Y(Y-1)-4R(R+1)L(L+1)}{2(2L-1)(2R-1)(2L+3)(2R+3)}$$
$$-\frac{1}{2}\frac{e^2}{a_0^4}\langle vR\mid \alpha(A)\mid vR\rangle\frac{\frac{1}{2}[3n^2-L(L+1)]}{n^5(L+\frac{3}{2})(L+1)(L+\frac{1}{2})L(L-\frac{1}{2})}$$
$$-\frac{1}{3}\frac{e^2}{a_0^4}\langle vR\mid \gamma(A)\mid vR\rangle\frac{\frac{1}{2}[3n^2-L(L+1)]}{n^5(L+\frac{3}{2})(L+1)(L+\frac{1}{2})L(L-\frac{1}{2})}\frac{3Y(Y-1)-4R(R+1)L(L+1)}{2(2L-1)(2R-1)(2L+3)(2R+3)}\ ,$$

where

$$Y\equiv R(R+1)+L(L+1)-N(N+1)\ . \tag{11}$$

Thus only three constants, the vibrationally averaged values of the quadrupole moment and the two polarizabilities, are required to calculate the first-order energies. Perturbations towards case-*b* coupling can be considered by calculating the effects of the off-diagonal matrix elements in Eqs. (9) and (10). This calculation has been performed numerically for the 4*d* states and is described in Sec. II F below.

E. Electric dipole matrix elements in case *d*

Using the explicit expressions for the case-*d* wave functions and their admixtures developed in Sec. II D, it is fairly easy to find the electric dipole transition amplitudes between Rydberg states. The required matrix elements are those of the operator[15]

$$\hat{e}\cdot\vec{Q}_{\rm el}^{(1)}\ , \tag{12}$$

where $\tilde{Q}$ denotes the electric dipole of the molecule and $\hat{e}$ is a unit vector specifying the electric field direction. Specializing to the case of the molecular Rydberg states, the dipole operator has the form

$$Q_M^{(1)}({\rm el})=-erC_M^{(1)}(\theta,\phi)+\sum_{\rm core}q_{\rm core}r_{\rm core}C_M^{(1)}(\theta_{\rm core},\phi_{\rm core})+\mu_M\ , \tag{13}$$

where μ is induced by polarizability. Here $(\theta_{\rm core},\phi_{\rm core})$ are the coordinates of the core particles in the laboratory-fixed frame, and the sum is over all three particles of the H_2^+ core. The portion of Q arising from the core polarizability can be written in terms of the isotropic and anisotropic polarizabilities using the methods developed above with the result

$$Q_M^{(1)}({\rm el})=-erC_M^{(1)}(\theta,\phi)+\sum_{\rm core}e_{\rm core}r_{\rm core}C_M^{(1)}(\theta_{\rm core},\phi_{\rm core})$$
$$+\frac{c}{r^2}(\alpha-\tfrac{1}{3}\gamma)C_M^{(1)}(\theta,\phi)+\frac{e}{r^2}\gamma[\vec{\vec{C}}^{(1)}(\theta,\phi)\cdot\vec{\vec{C}}^{(1)}(\theta_c,\phi_c)]C_M^{(1)}(\theta_c,\phi_c)\ . \tag{14}$$

The first term is the only one that need normally be considered. The second term does not contribute so long as the vibrational motion is separable, though for a heteronuclear molecule it is the term giving rise to pure rotational and vibrational transitions. The last two terms describe transitions arising from the admixture of core wave functions by the polarizability of the core and are significant only when deviations from Hund's case *d* are large. For the first term, the *M*th component of the matrix element can be determined using the same angular momentum methods employed above, giving

$$(\langle v'R'n'L'N'M_N'\mid \hat{e}\cdot\vec{Q}_{\rm el}^{(1)}\mid vRnLNM_N\rangle)_M=-e_Me\langle n'L'\mid r\mid nL\rangle(-1)^{N'-M_N'}\begin{pmatrix}N' & 1 & N\\ -M_N' & M & M_N\end{pmatrix}$$
$$\times(-1)^{R+L+N'+1}\sqrt{(2N+1)(2N'+1)}\begin{Bmatrix}L' & N' & R\\ N & L & 1\end{Bmatrix}$$
$$\times(-1)^{L'}\sqrt{(2L+1)(2L'+1)}\begin{pmatrix}L' & 1 & L\\ 0 & 0 & 0\end{pmatrix}\langle v'\mid v\rangle\ . \tag{15}$$

The resulting selection rules for electric dipole transitions are

$$\Delta M_N = 0, \pm 1,$$
$$\Delta N = 0, \pm 1 \text{ (but not } N=0 \rightarrow N=0),$$
$$\Delta L = \pm 1,$$
$$\Delta R = 0,$$
$$\Delta v = 0.$$

The selection rule for the vibrational quantum number is not rigorous, and off-diagonal transitions are allowed to the extent that the vibrational overlap integrals are nonzero, or the core polarizability and quadrupole moments cause admixtures of different vibrational levels.

The radiative decay rate of a Rydberg state can be obtained easily from the dipole matrix elements (15). The Einstein A coefficient is given by

$$A = \frac{4k^3}{3\hbar} e^2 (2N'+1)(2L+1)(2L'+1) \times \begin{Bmatrix} L' & 1 & L \\ 0 & 0 & 0 \end{Bmatrix}^2 \begin{Bmatrix} L' & N' & R \\ N & L & 1 \end{Bmatrix}^2 |\langle v' | v \rangle|^2 . \quad (16)$$

Here the primes refer to the lower state for a particular transition with wave vector K. An interesting property of Eq. (16) is that, if it is summed over all values of N', the orthogonality property of the 6-j symbols shows that the lifetime is independent of N. This is not surprising, since the effects of an external field should not depend upon the orientation of the core rotation angular momentum vector $\vec{R}$.

F. Application to the 4*d* states

Because the 4*d* states exhibit a considerable amount of intermediate coupling, it is necessary to consider both the diagonal and off-diagonal matrix elements of the perturbations described in Sec. II C. This section describes the procedure used to obtain approximate theoretical energies for these states, starting with published theoretical data for the H_2^+ molecular ion. A brief summary of this procedure is given below, followed by a more detailed description of each step.

(1) Theoretical values of the quadrupole moment and polarizability of H_2^+ were taken from the literature for each of several static values of the internuclear separation A.

(2) For each choice of the rotational and vibrational quantum numbers, rotationally averaged values of the polarizability and quadrupole moment were found by numerical integration.

(3) Zeroth-order energies were obtained for each level using published values for the rotational and vibrational energy levels of the H_2^+ ion and purely hydrogenic values for the binding energy of the Rydberg electron.

(4) Perturbation matrices were set up for the first several rotational levels of each state. These matrices were diagonalized numerically to give the predicted energy levels. These energies are compared with experimental values in Sec. IV below.

The quadrupole moment of H_2^+ was calculated at various fixed internuclear separations by Karl, Nickel, Poll, and Wolniewicz.[16] This result is quite accurate since it depends only on a numerical integration over the well-known ground-state wave functions. The static polarizabilities were taken from an article by Sherstyuk and Yakovleva,[17] who incorporated continuum contributions by expanding the two-center Green's function in a basis set of Sturm functions that have a purely discrete spectrum. These polarizabilities and quadrupole moments were least-squares fitted to power series of low order to provide accurate interpolation and a small extrapolation beyond the last polarizability point calculated at an internuclear separation of 3.4 a.u.

An approximation was then made by numerically integrating these power series over the rovibrational wave functions of unperturbed H_2^+ to give averaged values of the interaction constants. This is equivalent to assuming that the core constants are not significantly affected by the fact that the admixture of core basis states differs slightly with internuclear separation. The core wave functions were obtained by numerical methods, using as input the eigenvalues and potential curves tabulated by Hunter, Yau, and Pritchard,[18] and using Numerov integration[19,20] to solve Schrödinger's equation separately for the potential of each rovibrational level. After averaging over these wave functions, the constants show a weak dependence on the rotational quantum number but a much stronger dependence on the vibrational level. A feeling for this dependence can be obtained by examining the results for a few sample levels, given in Table I.

A large number of digits are shown only to make the rotational dependence apparent. These values are accurate to only within a few percent, due to numerical errors and the slight sensitivity of the averaged polarizabilities to the values of the fixed-separation polarizabilities for larger internuclear separations than given in Ref. 17.

The energy levels of Hunter, Yau, and Pritchard[18] were used again to obtain the zeroth-order energies.

TABLE I. Dependence of the calculated polarizability and quadrupole moment on the rotational and vibrational quantum numbers. Results are expressed in a.u.

v	R	α	γ	Q
0	0	3.103	3.906	1.650
0	1	3.106	3.914	1.651
0	2	3.126	3.954	1.659
0	3	3.155	4.015	1.672
1	0	3.825	5.587	1.884
2	0	4.744	7.851	2.127
3	0	5.924	10.867	2.387

The binding energy of the outer electron was calculated using a mass-corrected value for the Rydberg constant of 109 707.45 cm^{-1}. Finally, the perturbation matrices were diagonalized to calculate the actual energies. The first six rotational levels of each state were included in the calculation, but perturbations between states of different n or L were not included.

In Sec. IV of this paper, calculated energies for a large number of 4d states are compared with the present experiment and with older spectroscopic data. The results are surprisingly close to the actual energy levels, considering the simplicity of the model. To gain an understanding of the magnitudes of the various effects, it is useful to examine a typical state. For the $v=0$, $N=2$ level of parahydrogen in the $4d\ ^3\Delta_g$ state, the hydrogenic binding energy of the Rydberg electron is -7042.75 cm^{-1} and the zeroth-order rotational and vibrational energy is 575.47 cm^{-1}. The diagonal polarization interaction lowers the energy by 107.23 cm^{-1}, the diagonal quadrupole interaction lowers it by a further 78.81 cm^{-1}, and perturbative mixing with the $R=0$ and 4 basis states raises the energy by 9.3 cm^{-1}. The result is an energy of 117 959.20 cm^{-1} expressed relative to the $v=0$, $N=0$ level of the ground state of H_2. This is fortuitously close to the experimentally determined value of 117 958.58 cm^{-1}. More typically, the result differs by about ten wave numbers from experiment. It should be emphasized that the sizes of the various corrections differ considerably from level to level and that the quadrupole and perturbation corrections can be of either sign.

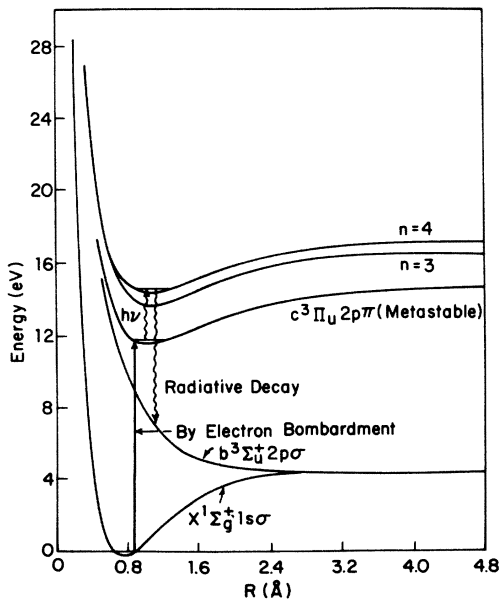

FIG. 4. Energy-level diagram showing the scheme for excitation and observation of the $n=4$ triplet states. Potentials are taken from Ref. 25.

III. OBSERVATION OF THE 4s AND 4d STATES

The experimental arrangement has been described elsewhere.[21] Figure 4 shows a schematic diagram of the manner in which the states were excited and their decay observed. The experiment described here is essentially a survey at modest resolution, undertaken because the existing identifications of transitions to triplet $n=4$ states are incomplete and somewhat unreliable. The region from 22 072 to 22 607 cm^{-1} has been searched exhaustively at a resolution of about 100 MHz, and a number of isolated regions to either side were examined in an attempt to find particular transitions. While this by no means exhausts the list of transitions to 4d and 4s that can be observed with the present apparatus, it provides a sufficiently extensive list of lines to permit unambiguous identifications for transitions to the lower vibrational and rotational levels. For the 4d states, it has been possible to observe transitions from the first several rotational levels of the $v=0$, $v=1$, and $v=2$ vibrational levels. A few transitions with $v=3$ have also been identified, although a systematic study of these levels has not been attempted.

The searching process was complicated somewhat because the single-mode dye laser cannot perform continuous scans over a range wider than 40 GHz. As a result it was necessary to perform a great many separate scans, resetting the laser frequency manually after each scan. Each region was initially examined at a rapid scan rate, so that a 1-cm^{-1} interval could be covered in a few minutes. The Channeltron output signal was recorded together with the absorption spectrum of tellurium dimers on a chart recorder, and the resulting trace was examined for evidence of transitions. If no transitions were

TABLE II. Complete list of the observed transitions, showing assignments where they have been made. Strengths should be taken only as a qualitative indication since no attempt has been made to correct for laser intensity variations or detection efficiency.

Frequency (cm^{-1})	Strength	Upper state and branch	Frequency (cm^{-1})	Strength	Upper state and branch
21 918.885	0.3	$4d\ \Pi$, $v=2$, $P(4)$	22 438.042	0.4	$4s\ \Sigma$, $v=1$, $Q(1)$
22 031.317	1.4	a, ortho	22 453.104	1.5	$4d\ \Pi$, $v=1$, $R(4)$
22 033.001	0.7	$4d\ \Pi$, $v=2$, $P(3)$	22 455.771	1.5[b]	$4d\ \Delta$, $v=3$, $R(2)$
22 073.427	6.1	$4d\ \Sigma$, $v=2$, $Q(1)$	22 466.053	2.1	$4d\ \Pi$, $v=1$, $R(3)$
22 080.766	0.6	a, para	22 468.151	0.2	$4d\ \Pi$, $v=1$, $Q(5)$
22 081.173	0.9	a, para	22 477.594	2[b]	$4d\ \Pi$, $v=1$, $R(2)$
22 092.187	1.1	a, ortho	22 478.072	5.0	$4d\ \Sigma$, $v=0$, $Q(1)$
22 099.046	2.6	a, para	22 481.737	0.5	$4d\ \Pi$, $v=1$, $Q(4)$
22 100.815	3.4	a, ortho	22 487.002	4.3	$4d\ \Delta$, $v=2$, $Q(2)$
22 114.576	0.3	$4d\ \Delta$, $v=3$, $P(3)$	22 489.686	5.8	$4d\ \Pi$, $v=1$, $R(1)$
22 116.973	0.1	a, ortho, broad	22 494.891	1.6	$4d\ \Pi$, $v=1$, $Q(3)$
22 149.763	5.2	$4d\ \Pi$, $v=2$, $P(2)$	22 501.772	3.1	$4d\ \Pi$, $v=1$, $Q(2)$
22 171.179	2.8	$4d\ \Sigma$, $v=1$, $Q(2)$	22 525.333	4.9	$4d\ \Pi$, $v=0$, $P(2)$
22 202.490	1.8	a, ortho	22 532.718	0.6	a, para
22 203.168	0.3	$4d\ \Pi$, $v=1$, $P(3)$	22 533.092	0.9	$4d\ \Delta$, $v=3$, $R(3)$
22 230.382	0.5	$4d\ \Sigma$, $v=0$, $Q(3)$	22 535.582	0.7	$4s\ \Sigma$, $v=0$, $Q(4)$
22 241.102	0.3	$4d\ \Delta$, $v=2$, $P(5)$	22 541.726	0.8	$4s\ \Sigma$, $v=0$, $Q(3)$
22 260.069	0.7	$4d\ \Pi$, $v=2$, $R(5)$[a]	22 545.361	8.7	$4d\ \Delta$, $v=2$, $R(1)$
22 261.271	1.2	$4d\ \Delta$, $v=2$, $P(4)$	22 547.280	2.2	$4s\ \Sigma$, $v=0$, $Q(2)$
22 269.357	1.8	a, para	22 557.732	0.3	$4s\ \Sigma$, $v=0$, $Q(1)$
22 270.755	0.4	$4s\ \Sigma$, $v=2$, $Q(5)$[a]	22 566.861	1.1	$4d\ \Pi$, $v=1$, $Q(1)$
22 272.695	1.0	$4d\ \Delta$, $v=2$, $P(3)$	22 571.807	0.5	$4d\ \Delta$, $v=2$, $Q(3)$
22 275.302	1.5	one is $4s\ \Sigma$, $v=2$, $Q(4)$	22 587.983	0.8	$4d\ \Delta$, $v=0$, $P(3)$
22 276.955	1.2	other is $4d\ \Pi$, $v=2$, $R(4)$	22 604.571	0.2	$4d\ \Pi$, $v=0$, $R(5)$
22 284.980	6.3	$4d\ \Sigma$, $v=1$, $Q(1)$	22 619.001	1.1	$4d\ \Pi$, $v=0$, $R(4)$
22 287.777	3.3	$4d\ \Pi$, $v=2$, $R(3)$	22 624.943	0.1	$4d\ \Pi$, $v=0$, $Q(5)$
22 289.688	0.9	$4s\ \Sigma$, $v=2$, $Q(3)$	22 631.759	2.2	$4d\ \Pi$, $v=0$, $R(3)$
22 291.419	2.9	$4d\ \Delta$, $v=3$, $Q(2)$[a]	22 637.434	0.7	$4d\ \Pi$, $v=0$, $Q(4)$
22 297.676	8	$4d\ \Pi$, $v=2$, $R(2)$	22 640.061	6.8	$4d\ \Delta$, $v=2$, $R(2)$
22 298.133	2.7	$4s\ \Sigma$, $v=2$, $Q(2)$	22 643.773	3[b]	$4d\ \Pi$, $v=0$, $R(2)$
22 305.666	5[b]	$4d\ \Pi$, $v=2$, $R(1)$	22 647.775	0.7	$4d\ \Pi$, $v=0$, $Q(3)$
22 316.985	0.2	$4s\ \Sigma$, $v=2$, $Q(1)$[a]	22 648.369	0.7	$4d\ \Delta$, $v=2$, $Q(4)$
22 331.585	0.8	$4d\ \Pi$, $v=2$, $Q(4)$[a]	22 656.651	2.3	$4d\ \Pi$, $v=0$, $Q(2)$
22 333.278	0.7	a, ortho	22 657.864	6.3	$4d\ \Pi$, $v=0$, $R(1)$
22 335.808	2.9	$4d\ \Pi$, $v=2$, $Q(3)$	22 690.817	1.5	$4d\ \Delta$, $v=1$, $Q(2)$
22 343.804	4.8	$4d\ \Pi$, $v=1$, $P(2)$	22 716.679	2.3	$4d\ \Delta$, $v=1$, $R(1)$
22 344.823	5.6	$4d\ \Pi$, $v=2$, $Q(2)$	22 723.179	1.3	$4d\ \Delta$, $v=2$, $R(3)$
22 354.020	0.9	$4d\ \Delta$, $v=3$, $Q(3)$[a]	22 772.215	0.8	$4d\ \Pi$, $v=0$, $Q(1)$
22 355.310	1.0[b]	$4d\ \Sigma$, $v=0$, $Q(2)$	22 795.401	0.2	$4d\ \Delta$, $v=1$, $Q(3)$[a]
22 357.062	0.3	$4d\ \Pi$, $v=0$, $P(3)$	22 830.534	1.7	$4d\ \Delta$, $v=1$, $R(2)$
22 361.207	1.6	$4d\ \Pi$, $v=2$, $Q(1)$	22 888.773	2.4	$4d\ \Delta$, $v=0$, $R(1)$
22 373.742	4.5	$4d\ \Delta$, $v=3$, $R(1)$	22 896.071	1[b]	$4d\ \Delta$, $v=0$, $Q(2)$
22 405.67	0.2	$4s\ \Sigma$, $v=1$, $Q(5)$	22 924.670	0.7	$4d\ \Delta$, $v=1$, $R(3)$
22 414.425	1.6	$4s\ \Sigma$, $v=1$, $Q(4)$	23 001.422	0.5	$4d\ \Delta$, $v=0$, $Q(3)$
22 420.980	1.0	$4s\ \Sigma$, $v=1$, $Q(3)$	23 004.815	2	$4d\ \Delta$, $v=0$, $R(2)$
22 427.450	2.6	$4s\ \Sigma$, $v=1$, $Q(2)$	23 110.603	0.4	$4d\ \Delta$, $v=0$, $R(3)$
22 430.162	0.8	$4d\ \Delta$, $v=1$, $P(3)$			

[a]These assignments are uncertain.

[b]These lines were observed under unusual conditions, and the strengths are particularly inaccurate.

found, the tellurium spectrum was used to ascertain that adjacent scans overlapped by a suitable amount. If a transition appeared to be present, it was reexamined with a parahydrogen gas source in place of the usual natural hydrogen to determine to which species the transition belonged. A slower scan was then taken over a region centered about the transition, and a microcomputer system was used to acquire simultaneously the H_2 spectrum, the tellurium absorption spectrum, and the fringes from a $\frac{1}{2}$-m reference interferometer. Since the signals are for the most part quite strong, the entire experiment occupied only a few hundred hours of running time.

Table II presents a complete list of the observed transitions. As described in Ref. 5, the absorption spectrum of tellurium dimers has been used to determine the frequency of each transition. Since much of the fine and hyperfine structure is unresolved at the resolution of about 100 MHz used for this work, the frequencies have been measured to the peak of the largest component observed for each transition without regard to the identity of this component. The accuracy of the absolute wavelengths is limited primarily by the accuracy of the tellurium atlas[22] and is presumably at least as good as the 0.006 cm^{-1} claimed for the initial version of the iodine atlas prepared by the same group.[23] The other columns of Table II give the line assignments as described in Sec. IV of this paper and the approximate signal strengths, in thousands of counts per second observed on the Channeltron detector. These signal sizes should be used only for qualitative purposes, since no attempt was made to correct for the large day-to-day variations in laser power and alignment conditions. Transitions to states with $v > 1$ show an enhancement in signal size, one of a number of peculiarities arising because they decay primarily by predissociation.

The discovery that the 4s and 4d states with $v > 1$ are predissociative was somewhat serendipitous. It was found early in the course of the experiment that a number of extraordinarily strong lines were present, many at frequencies where transitions are weak or absent in the molecular-hydrogen wavelength table compiled by Crosswhite.[4] When narrow collimating slits were placed in the apparatus to narrow the experimental bandwidth to a few tens of megahertz, it was found that these lines had a natural width far in excess of what was expected. The widths of several hundred megahertz observed for most of these states imply lifetimes of roughly 500 psec. This is far shorter than the radiative lifetimes expected for $n = 4$ states, which are more typically tens of nanoseconds. The $n = 4$ states are not sufficiently energetic to autoionize, so predissociation is the only possible channel for rapid decay. The Channeltron is more sensitive both to Lyman-α radiation and to metastable particles than to the longer-wavelength ultraviolet light by which radiating states are observed. Thus a predissociation into a ground-state hydrogen atom and a hydrogen atom in either the 2s or the 2p state would explain the anomalously large signals as well. In retrospect it should not have been surprising to see predissociation for these states, since evidence for predissociation has been found for levels of the $h\,^3\Sigma_g^+\,3s\sigma$ state having $v \geq 3$.[24]

Figure 5 shows the molecular potentials involved in the predissociation process. The $n = 4$ potential shown is approximate; the exact potentials have apparently never been calculated. In any case, the potentials for all of the $n = 4$ states would not perceptibly differ from one another for small internuclear separations. The other potentials are taken from Ref. 25. The $v = 0$ levels are below the H 1s + H 2s or 2p predissociation threshold, in accord with the experimental observation that they are all long lived. For higher levels, allowed predissociation is possible by coupling with the vibrational continua of the lower potentials shown in Fig. 5. A poor vibrational overlap with the $2s\,^3\Sigma_g^+$ state is expected because its potential curve lies far from the $n = 4$ potentials at small internuclear separations. At larger separations the continuum vibrational wave functions oscillate rapidly, and as a result the vibrational overlap in-

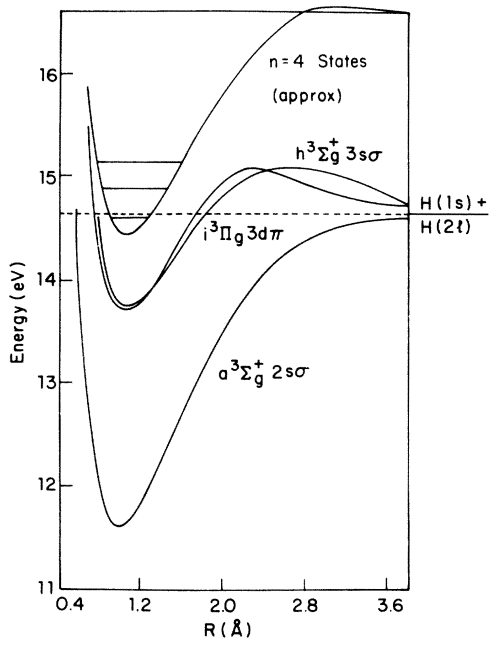

FIG. 5. Energy-level diagram showing the levels involved in the predissociation of $4s\,^3\Sigma_g^+$. Potentials for the $n = 3$ and 4 states were taken from Ref. 25.

tegral tends to cancel almost completely. This leaves the $h\,^3\Sigma_g^+\,3s\sigma$ and $i\,^3\Sigma_g^+\,3d\sigma$ potentials as the most likely predissociation paths. For levels with $v=1$ this process is likely to be suppressed because the potentials for both $h\,^3\Sigma_g^+\,3s\sigma$ and $i\,^3\Sigma_g^+\,3d\sigma$ exhibit large humps that rise well above the energy of the $n=4$ states. Only nonadiabatic mixings could allow these levels to predissociate. By contrast, the $v=2$ levels lie slightly above both humps and are free to decay.

In agreement with this discussion, there is no experimental evidence for predissociation of the $v=1$ levels. The $v=2$ and 3 levels appear to be predissociative without exception. Observed linewidths range from about 100 MHz to about 1 GHz and seem to vary rather erratically from level to level. A systematic study of the predissociation lifetimes has yet to be undertaken. Because the natural linewidth is of the same order of magnitude as the fine- and hyperfine-structure splittings, accurate determinations of the lifetimes will require a careful treatment of line-shape distortion caused by the blending of the several components of each transition.

A simple experiment was performed to ascertain that predissociation was actually occurring and to determine whether the resulting excited hydrogen atoms are in the $2s$ or the $2p$ state. This consisted of placing two different windows over the Channeltron detector, which is sensitive both to vacuum ultraviolet light and to metastable species. The first was made of CaF_2 and showed a sharp cutoff at about 1250 Å. As a result this window blocked both metastable particles and Lyman-α radiation but transmitted the bulk of the radiative decay light by which nondissociative states are observed. A small selection of transitions was examined with this window in place. Transitions to the $v=0$ and 1 levels were diminished only slightly, but transitions to the higher vibrational levels became entirely unobservable. The second window was made of MgF_2, which transmits fairly well at Lyman-α. If the predissociation were to H $2s$ the signals would still be unobservable because the metastables would be blocked. Instead, the transitions were diminished only by about a factor of 2, consistent with a signal resulting entirely from Lyman-α radiation emitted by decaying H $2p$ atoms. This experiment was conducted with grounded grids placed above the detector to rule out the possibility that metastable hydrogen might be quickly quenched due to Stark mixing by static electric fields.

IV. LINE ASSIGNMENTS AND COMPARISON WITH THEORY

Because of the large rotational constant of H_2, its spectrum shows no sign whatever of macroscopic ordering at first glance. Matters are further complicated for the $4d$ states because they exhibit intermediate coupling. In either the case-b or the case-d basis set the extent of perturbative admixture varies erratically from level to level, making it impossible to fit the observed spectra to a simple rotational progression. In view of these difficulties it is hardly surprising that some of the line assignments made by Richardson and others[1–3] were erroneous. Since they were faced with an extremely dense optical spectrum and proceeding without the assistance of a quantitative theoretical calculation, it is remarkable that most of their work has withstood the test of later scrutiny as well as it has.

Several factors have combined to make the identification process far easier for the work reported here. The only transitions observable are those to the $4s$ and $4d$ states, vastly reducing the number of lines to be sorted out. In most cases it is possible to identify the vibrational quantum number from the appearance of the transition, as described below. Nearly as important is the availability of a reasonably accurate *ab initio* theory with which the observed spectra can be compared. Another advantage is that predissociative levels can be observed easily using the Channeltron detector. These transitions were weak or absent in earlier optical emission spectra, further complicating the identification problem. One drawback of the new approach is that it is difficult in many cases to find combinations for which more than one transition terminates on the same rotational level. This peculiarity arises because the $c\,^3\Pi_u\,2p\pi$ state is metastable only for parahydrogen levels of even N and for orthohydrogen levels of odd N.[26] For those $4s$ and $4d$ levels to which a Q branch is seen, the lower levels required for P and R branches simply do not exist in the beam. For the same reason the $N=0$ levels of Σ states cannot be seen at all, since a P branch from an odd level of orthohydrogen would be the only possible transition.

At the 100-MHz resolution used for this survey, it is usually possible to identify the vibrational level uniquely from the appearance of the fine structure. Because the fine structure of the upper state is always small compared with that of the lower state, the observed lines tend to exhibit three clumps of components corresponding to the lower-state structure, one of them considerably removed from the other two. The relative size of this third component diminishes rapidly as the vibrational number increases. The apparent cause is that the fine-structure sublevel of the metastable state with $J=N$ has a shorter lifetime than the other sublevels, and not all of the metastables of this type survive the transit time from beam source to interaction region. This effect has been verified by calculation for the

metastable parahydrogen levels with $N=2$,[27] and was seen experimentally for the same lower levels in the $3s,3d$ spectra observed by Lichten and Wik.[28] With the 10-cm transit distance used for the experiment reported here, the "suppressed" fine-structure components were diminished little from their statistical intensities for $v=0$, but were reduced roughly by a factor of 5 for $v=1$, and were altogether invisible for higher v. An independent check for levels with $v=2$ and higher was afforded because these levels invariably give the strong, broadened lines characteristic of predissociation.

With the aid of these clues, the transitions were assigned on the basis of several criteria. The following characteristics were sought for a good assignment.

(1) A good match with the results of the theoretical model. For rotational levels with $N=2$ and higher, a repeating pattern of deviations from the model is usually seen. For example, all of the Q branches to $4d\Pi$ with $v=0$ show a difference from the model of about -7.5 cm^{-1}, and all of the P and R branches show a difference of about -10 cm^{-1}. Thus the model has useful predictive power at the level of 1 cm^{-1} or less, even though its absolute accuracy is an order of magnitude worse.

(2) Where possible, confirming combinations. In those cases where P and R branches could be both observed, there can be no doubt about the correctness of the assignments. The slight combination defects shown in Tables III–V result from small errors in the metastable energy levels given by Dieke, which were used to determine the theoretical frequencies. In no case do these defects exceed 0.1 cm^{-1}.

(3) Agreement with the assignments given in Dieke. Failing this, it was usually possible to find one or more combinations in the hydrogen-molecule wavelength table prepared from his data. Such combinations are very helpful but not definitive by themselves, since the emission spectrum is so dense that apparent combinations frequently occur by accident. It was presumably by this means that incorrect assignments were originally made for some of the transitions.

(4) A reasonable line strength. Examination of the tables of assignments shows that in most cases, a repeating pattern of intensities is observed for the various branches that varies only slowly with rotational and vibrational number. The major discrepancy is a tendency to observe a sudden step for $v=2$, where the means of detection switches from radiative decay light to predissociation products. A quantitative treatment of the intensities was not attempted because the experimental intensities are quite crude and because the competition of various decay channels makes accurate calculation of the line strengths quite difficult.

Tables III–V provide a complete summary of the results for the $4d$ states. Only those transitions that could in principle be observed in the beam experiment are listed. Entries for $v=3$ are provided only

TABLE III. Transitions to the $4d\ ^3\Sigma_g^+$ state.

Branch	Theory (cm^{-1})	Dieke	Theory − Dieke	Experiment	Theory − Experiment	Strength	Notes
$v=0$, $Q(1)$	22 494.18	22 476.10	18.08	22 478.072	16.11	5	a
$v=0$, $Q(2)$	22 361.49	22 357.05	4.44	22 355.310	6.18	1.0	a,b
$v=0$, $Q(3)$	22 234.70	22 230.30	4.40	22 230.382	4.32	0.5	
$v=0$, $Q(4)$	22 109.15	22 105.81	3.34				
$v=1$, $Q(1)$	22 303.36	22 284.94	18.42	22 284.980	18.38	6.3	
$v=1$, $Q(2)$	22 182.13	22 171.15	10.98	22 171.179	10.95	2.8	
$v=1$, $Q(3)$	22 061.98	22 054.06	7.92				
$v=1$, $Q(4)$	21 942.04	21 936.21	5.83				
$v=1$, $Q(5)$	21 823.60	21 817.69	5.91				
$v=2$, $Q(1)$	22 098.79	22 073.37	25.42	22 073.427	25.36	6.1	
$v=2$, $Q(2)$	21 987.92	21 970.31	17.61				
$v=2$, $Q(3)$	21 874.52	21 861.44	13.08				
$v=2$, $Q(4)$	21 761.56	21 748.63	12.93				
$v=2$, $Q(5)$	21 646.55	21 631.13	15.42				

[a]Assignment differs from that given by Dieke.

[b]Line strength is particularly uncertain for these lines because they were taken under unusual conditions.

TABLE IV. Transitions to the $4d\ ^3\Pi_g$ state.

Branch	Theory (cm^{-1})	Dieke	Theory − Dieke	Experiment	Theory − Experiment	Strength	Notes
$v=0$, $Q(1)$	22 774.38			22 772.215	2.17	0.8	a
$v=0$, $P(2)$	22 517.93	22 501.74	16.19	22 525.333	−7.40	4.9	a
$v=0$, $Q(2)$	22 648.89	22 656.62	−7.73	22 656.651	−7.76	2.3	
$v=0$, $R(1)$	22 648.68	22 657.82	−9.14	22 657.864	−9.18	6.3	
$v=0$, $P(3)$	22 347.90	22 357.05	−9.15	22 357.062	−9.16	0.3	
$v=0$, $Q(3)$	22 640.40	22 647.74	−7.34	22 647.775	−7.38	0.7	
$v=0$, $R(2)$	22 634.19	22 643.74	−9.55	22 643.773	−9.58	3	b
$v=0$, $P(4)$	22 216.35	22 225.87	−9.52				
$v=0$, $Q(4)$	22 630.25	22 637.46	−7.21	22 637.434	−7.18	0.7	
$v=0$, $R(3)$	22 621.70	22 631.75	−10.05	22 631.759	−10.06	2.2	
$v=0$, $P(5)$	22 089.79	22 099.73	−9.94				
$v=0$, $Q(5)$	22 617.79	22 624.93	−7.14	22 624.943	−7.15	0.1	
$v=0$, $R(4)$	22 608.55	22 618.99	−10.44	22 619.001	−10.45	1.1	
$v=0$, $P(6)$	21 966.41	21 976.78	−10.37				
$v=0$, $R(5)$		22 604.56		22 604.571			
$v=1$, $Q(1)$	22 570.26	22 481.70	88.56	22 566.861	3.40	1.1	a
$v=1$, $P(2)$	22 333.30	22 332.81	0.49	22 343.804	−10.50	4.8	a
$v=1$, $Q(2)$	22 492.03	22 489.63	2.40	22 501.772	−12.14	3.1	a
$v=1$, $R(1)$	22 477.16	22 489.63	−12.47	22 489.686	−12.53	5.8	
$v=1$, $P(3)$	22 190.68	22 203.15	−12.47	22 203.168	−12.49	0.3	
$v=1$, $Q(3)$	22 481.58	22 494.85	−13.27	22 494.891	−13.31	1.6	
$v=1$, $R(2)$	22 464.13	22 477.49	−13.36	22 477.594	−13.46	2	b
$v=1$, $P(4)$	22 066.14	22 079.32	−13.18				

for the $4d\ ^3\Delta_g$ state, since it is only for this state that assignments to $v=3$ have so far been made. The first entry of each table gives the results of the theoretical calculation described in Sec. II. The transition frequencies were calculated by using the energies given by Dieke for the levels of the metastable $c\ ^3\Pi_u\ 2p\pi$ state, after making a correction of -149.6 cm^{-1} as determined by Miller and Freund.[29] The wavelength given by Dieke follows for those levels given assignments by him. The difference between the model and Dieke's data follows. The results of the present experiment are given next, together with the difference between the theoretical results and these new measurements. The final column gives line strengths in the same units as Table II.

In nearly all cases, more than one of the criteria listed above was satisfied. The letters in the Notes column are related to the footnotes and are used to denote those assignments that are subject to considerable doubt or to denote the levels for which the new results unambiguously differ from the old assignments. Table II shows a clump of unassigned lines near 22 100 cm^{-1}. Most of them undoubtedly belong to $v=3$ of the $4d\ ^3\Pi_g$ state and to $v=3$ of the $4s\ ^3\Sigma_g^+$ state, but there is at present not enough information to sort them out. The pattern of disagreements between the new and old assignments is somewhat peculiar. The first few rotational levels apparently caused particular difficulty for earlier investigators, perhaps because the rotational pattern characteristic of pure Hund's case d was being sought. The Q branches to $v=1$ of $4d\Pi$ were missed by large amounts with the exception of $Q(3)$, and the discrepancy between the old and new assignments reaches a rather startling 85 cm^{-1} for the $Q(1)$ branch. It is amusing that the transition previously assigned to $Q(1)$ turns out to be a parahydrogen transition and is in fact the $Q(4)$ branch to the same electronic and vibrational state. It is less

TABLE IV. (*Continued.*)

Branch	Theory (cm^{-1})	Dieke	Theory − Dieke	Experiment	Theory − Experiment	Strength	Notes
$v=1$, $Q(4)$	22 469.64	22 498.67	−29.03	22 481.737	−12.10	0.5	a
$v=1$, $R(3)$	22 452.28	22 466.03	−13.75	22 466.053	−13.77	2.1	
$v=1$, $P(5)$	21 945.60	21 959.19	−13.59				
$v=1$, $Q(5)$	22 455.00	22 498.67	−43.67	22 468.151	−13.15	0.2	a
$v=1$, $R(4)$	22 438.34	22 451.12	−12.78	22 453.104	−14.76	1.5	a
$v=1$, $P(6)$	21 826.74	21 839.52	−12.78				a
$v=1$, $R(5)$		22 435.00		22 438.042		0.4	a
$v=2$, $Q(1)$	22 352.09	22 293.48	58.61	22 361.207	−9.12	1.6	a
$v=2$, $P(2)$	22 137.65	22 170.49	−32.84	22 149.763	−12.11	5.2	a,c
$v=2$, $Q(2)$	22 322.62	22 311.58	11.04	22 344.823	−22.20	5.6	a
$v=2$, $R(1)$	22 289.69	22 316.73	−27.04	22 305.666	−15.98	5	a,b
$v=2$, $P(3)$	22 017.12	22 043.94	−26.82	22 033.001	−15.88	0.7	a
$v=2$, $Q(3)$	22 311.02	22 327.07	−16.05	22 335.808	−24.79	2.9	a
$v=2$, $R(2)$	22 280.52	22 304.84	−24.32	22 297.676	−17.16	8	a
$v=2$, $P(4)$	21 901.76	21 925.91	−24.15	21 918.885	−17.12	0.3	a
$v=2$, $Q(4)$	22 297.66	22 340.14	−42.48	22 331.585	−33.93	0.8	a,c
$v=2$, $R(3)$	22 268.92	22 289.62	−20.70	22 287.777	−18.86	3.3	a
$v=2$, $P(5)$	21 786.85	21 807.47	−20.62				a
$v=2$, $Q(5)$	22 282.65	22 350.66	−68.01				
$v=2$, $R(4)$	22 254.76	22 272.64	−17.88	22 275.302	−20.54	1.5	a,d
				or 22 276.955	−22.20	1.2	
$v=2$, $P(6)$	21 672.95	21 690.92	−17.97				a
$v=2$, $R(5)$		22 208.12		22 260.069		0.7	a,c

[a]Assignment differs from that given by Dieke.
[b]Line strength is particularly uncertain for these lines since they were observed under unusual conditions.
[c]Line assignment is not certain.
[d]One of these two lines is the desired $R(4)$ branch to $4d\ ^3\Pi_g$; the other is $Q(4)$ to $v=2$ of the $4s\ ^3\Sigma_g^+$ state.

surprising that all of the assignments to vibrational levels with $v>1$ that could be checked are erroneous. It was not previously suspected that these levels decay other than radiatively, so there would have been no reason to assign these transitions to emission lines that are weak or absent.

It was largely by a process of elimination that transitions were identified to a previously undiscovered state of Σ symmetry, presumably the triplet 4s state. The $v=0$ and 1 assignments to this state are quite firm, and the total absence of unassigned lines corresponding to P or R branches shows beyond any reasonable doubt that it is a Σ state. In fact, every observed line to the blue of 22 270 cm^{-1} has been assigned with the exception of the lines at 22 333.278 and 22 532.718 cm^{-1}. A separate publication gives a full report on the observation of this new state.[5]

The agreement with theory is excellent, considering that the calculation was a simple one containing no adjustable parameters. Agreement is frequently to within 10 cm^{-1}, although it becomes a bit worse for higher vibrational numbers where the deviation from hydrogenic energies is much larger. Only for the Q branches to $4d\Pi$ with $v=2$ does it exceed 30 cm^{-1}, and these are levels that appear to be perturbed significantly by the nearby $v=2$ levels of the 4s state. The fact that the deviations between experiment and theory tend to follow simple repeating patterns suggests that much of the discrepancy is

TABLE V. Transitions to the $4d\ ^3\Delta_g$ state.

Branch	Theory (cm^{-1})	Dieke	Theory − Dieke	Experiment	Theory − Experiment	Strength	Notes
$v=0$, $Q(2)$	22 896.69	22 895.98	0.71	22 896.071	0.62	1	a
$v=0$, $R(1)$	22 879.38	22 888.74	−9.36	22 888.773	−9.39	2.4	
$v=0$, $P(3)$	22 578.60	22 587.95	−9.35	22 587.983	−9.38	0.8	
$v=0$, $Q(3)$	23 002.80	23 001.34	1.46	23 001.422	1.38	0.5	
$v=0$, $R(2)$	22 995.49	23 004.65	−9.16	23 004.815	−9.33	2	
$v=0$, $P(4)$	22 577.65	22 586.85	−9.20				
$v=0$, $Q(4)$	23 098.85	23 130.53	−31.68				
$v=0$, $R(3)$	23 101.60	23 110.58	−8.98	23 110.603	−9.0	0.4	
$v=0$, $P(5)$	22 569.69	22 578.58	−8.89				
$v=0$, $Q(5)$	23 186.89	23 266.67	−79.78				
$v=0$, $R(4)$	23 199.35						
$v=0$, $P(6)$	22 557.21						
$v=1$, $Q(2)$	22 693.03			22 690.817	2.21	1.5	b
$v=1$, $R(1)$	22 705.16	22 716.71	−11.55	22 716.679	−11.52	2.3	
$v=1$, $P(3)$	22 418.68	22 430.09	−11.41	22 430.162	−11.48	0.8	
$v=1$, $Q(3)$	22 791.28			22 795.401	−4.12	0.2	b,c
$v=1$, $R(2)$	22 812.63	22 828.24	−15.61	22 830.534	−17.90	1.7	b
$v=1$, $P(4)$	22 414.64	22 430.09	−15.45				b
$v=1$, $Q(4)$	22 880.84						
$v=1$, $R(3)$	22 910.48	22 926.92	−16.44	22 924.670	−14.19	0.7	b
$v=1$, $P(5)$	22 403.80	22 420.29	−16.49				b

probably systematic in nature. No attempt has so far been made to alter the polarizabilities and quadrupole moments so as to attain a better fit, and it would not be surprising if some improvement could be realized. The deviations from hydrogenicity are sufficiently large that the neglect of higher-order moments may also be significant. One feature of the discrepancies that is poorly understood is the tendency for levels of very low N to deviate somewhat from the pattern of errors seen for higher levels. It is hoped that experiments on Rydberg states of high n can soon be performed, and it will be interesting to see whether these minor peculiarities recur for states lying much closer to pure case d.

V. CONCLUSION

The power of the laser-molecular beam approach has been clearly demonstrated by applying it to a poorly understood system of levels. Of the 93 transitions observed, all but 11 have been assigned, most with a high level of confidence. It proved possible to identify 14 transitions to a previously unknown state, thought to be $4s\ ^3\Sigma_g^+$. A number of discrepancies were found with the previous assignments to the $4d$ states. In particular, it appears that all transitions previously reported to vibrational levels with $v=2$ and higher are probably spurious. The absolute transition frequencies have been measured to about 0.006 cm^{-1}, limited only by the calibration of the frequency reference used. A simple theoretical approach based on the polarizability and quadrupole interactions of the Rydberg electron with the H_2^+ core gives results that agree remarkably well with the experimental energies.

It is hoped that more accurate theoretical treatments will be stimulated by this work. The success of the simple Rydberg-state model suggests that it might be improved further, perhaps by incorporating its results into a formalism such as multichannel quantum-defect theory that would include perturbations between levels of different n and L in a systematic fashion. It would be interesting to see how

TABLE V. (*Continued.*)

Branch	Theory (cm^{-1})	Dieke	Theory − Dieke	Experiment	Theory − Experiment	Strength	Notes
$v=2$, $Q(2)$	22 482.12	22 569.33	−87.21	22 487.002	−4.88	4.3	b
$v=2$, $R(1)$	22 527.09	22 541.70	−14.61	22 545.361	−18.27	8.7	b
$v=2$, $P(3)$	22 254.52	22 269.19	−14.67	22 272.695	−18.18	1	b
$v=2$, $Q(3)$	22 572.32	22 667.99	4.33	22 571.807	0.51	0.5	b
$v=2$, $R(2)$	22 623.92	22 651.45	−27.53	22 640.061	−16.14	6.8	b
$v=2$, $P(4)$	22 245.16	22 272.64	−27.48	22 261.271	−16.11	1.2	b
$v=2$, $Q(4)$	22 652.46	22 785.33	−132.87	22 648.369	4.09	0.7	b
$v=2$, $R(3)$	22 714.22	22 734.86	−20.64	22 723.179	−8.96	1.3	b
$v=2$, $P(5)$	22 232.15	22 253.37	−21.22	22 241.102	−8.95	0.3	b
$v=2$, $Q(5)$	22 723.95	22 903.43	−179.48				
$v=2$, $R(4)$	22 796.66						
$v=2$, $P(6)$	22 214.85						
$v=3$, $Q(2)$	22 273.92	22 396.73	−122.81	22 291.419	−17.50	2.9	b,c
$v=3$, $R(1)$	22 346.36	22 361.60	−15.24	22 373.742	−27.38	4.5	b
$v=3$, $P(3)$	22 087.18	22 102.09	−14.91	22 114.576	−27.40	0.3	b
$v=3$, $Q(3)$	22 346.78	22 495.41	−148.63	22 354.020	−7.24	0.9	b,c
$v=3$, $R(2)$	22 432.32	22 460.86	−28.54	22 455.771	−23.45	1.5	b,a
$v=3$, $P(4)$	22 072.28	22 100.78	−28.50				
$v=3$, $Q(4)$	22 415.48	22 604.56	−189.08				
$v=3$, $R(3)$	22 512.08	22 526.43	−14.35	22 533.092	−21.01	0.9	b
$v=3$, $P(5)$	22 054.05	22 068.37	−14.32				b
$v=3$, $Q(5)$	22 480.15						
$v=3$, $R(4)$	22 585.58						

[a]Line strength is particularly uncertain for these lines since they were observed under unusual conditions.
[b]Assignment differs from that given by Dieke.
[c]Line assignment is not certain.

such an approach would compare with the more traditional approach of calculating accurate molecular potentials in a case-*b*-like basis, then considering perturbations between them. A better understanding of the predissociation process would also be valuable, especially since many of the levels studied lie quite close to threshold, either just above or just below it.

Several further experiments are suggested by the results presented here. Comparison of D_2 spectra with the H_2 results could provide considerable insight regarding the remaining discrepancies between experimental- and theoretical-level positions. Other possibilities include fine-structure determinations, lifetime measurements, and a search for the predissociative $v=3$ levels of the $n=3$ states. Of particular interest is the spectroscopy of the higher Rydberg states. An experiment is presently in progress in which two dye lasers are used to achieve stepwise excitation of the *np* and *nf* Rydberg series. It is thought that states with principal quantum numbers ranging from about 7 on up to 30 or 40 will be observable. The goal will be to undertake a systematic study of both the level positions and the decay processes, especially the competition between autoionization, predissociation, and radiative decay.

ACKNOWLEDGMENTS

Professor Stephen Lundeen of Harvard University first suggested the polarizability-quadrupole moment approach and assisted us greatly in developing this model for the Rydberg states of H_2. This research was supported in part by National Science Foundation Grant No. PHY-80-26547.

[1]O. W. Richardson, *Molecular Hydrogen and its Spectrum* (Yale University Press, New Haven, Conn., 1934).
[2]O. W. Richardson, P. M. Davidson, J. Morsden, and W. M. Evans, Proc. R. Soc. London 142, 40 (1933).
[3]O. W. Richardson and T. B. Rymer, Proc. R. Soc. London 147, 24 (1934).
[4]H. M. Crosswhite, *The Hydrogen Molecule Wavelength Tables of Gerhard Heinrich Dieke* (Wiley-Interscience, New York, 1972).
[5]E. E. Eyler and F. M. Pipkin, J. Chem. Phys. 77, 5315 (1982).
[6]E. S. Chang and H. Sakai J. Phys. B 15, L649 (1982).
[7]G. Herzberg and Ch. Jungen, J. Chem. Phys. 77, 5876 (1982).
[8]P. M. Dehmer and W. A. Chupka, J. Chem. Phys. 65, 2243 (1976).
[9]M. Rothschild, H. Egger, R. T. Hawkins, J. Bokor, H. Pummer, and C. K. Rhodes, Phys. Rev. A 23, 206 (1981), and references therein.
[10]M. Raoult and Ch. Jungen, J. Chem. Phys. 74, 3388 (1981), and references therein.
[11]G. Herzberg and Ch. Jungen, J. Mol. Spectrosc. 41, 425 (1972).
[12]Jon T. Hougen, *The Calculation of Rotational Energy Levels and Rotational Line Intensities in Diatomic Molecules,* Natl. Bur. Stand. (U.S.) Monograph 115 (U.S. GPO, Washington, D. C., 1970).
[13]A. R. Edmonds, *Angular Momentum in Quantum Mechanics* (Princeton University Press, Princeton, N. J., 1974).
[14]K. B. MacAdam, Ph.D. thesis, Harvard University, 1971 (unpublished).
[15]M. Mizushima, *Quantum Mechanics of Atomic Spectra and Atomic Structure* (Benjamin, New York, 1970).
[16]G. Karl, B. Nickel, J. D. Poll, and L. Wolniewicz, Phys. Rev. Lett. 34, 1302 (1975).
[17]A. I. Sherstyuk and N. S. Yakovleva, Opt. Spektrosk. 40, 977 (1976) [Opt. Spectrosc. (USSR) 40, 560 (1976)].
[18]G. Hunter, A. W. Yau, and H. O. Pritchard, At. Data Nucl. Data Tables 14, 11 (1974).
[19]J. W. Cooley, Math. Comput. 15, 363 (1961).
[20]J. K. Cashion, J. Chem. Phys. 39, 1872 (1963).
[21]E. E. Eyler and F. M. Pipkin, Phys. Rev. Lett. 47, 1270 (1981); also Ref. 5.
[22]J. Cariou and P. Luc, Atlas du Spectre D'Absorption de la Molécule de Tellure, Labortoire Aimé-Cotton, Centre National de la Recherche Scientifique II, 91405 Orsay, France, 1980 (unpublished).
[23]S. Gerstenkorn and P. Luc, *Atlas du Spectre D'Absorption de la Molécule D'Iode* (CNRS, Paris, 1978). A systematic correction is described by S. Gerstenkorn and P. Luc, Rev. Phys. Appl. 14, 791 (1979).
[24]H. Beutler and H. O. Jünger, Z. Phys. 101, 285 (1936).
[25]T. E. Sharp, At. Data 2, 119 (1971).
[26]W. Lichten, Phys. Rev. A 4, 2217 (1971).
[27]L. Y. C. Chiu and D. K. Bhattacharyya, J. Chem. Phys. 70, 4376 (1979).
[28]W. Lichten, T. Wik, and T. A. Miller, J. Chem. Phys. 71, 2441 (1979).
[29]T. A. Miller and R. S. Freund, J. Chem. Phys. 61, 2160 (1974).